Density-functional study of homogeneous bubble nucleation in the stretched Lennard-Jones fluid

Vincent K. Shen and Pablo G. Debenedetti[a)]
Department of Chemical Engineering, Princeton University, Princeton, New Jersey 08544

(Received 6 October 2000; accepted 6 December 2000)

Density-functional theory is used to study homogeneous bubble nucleation in the stretched Lennard-Jones liquid. We show that the ratio of density-functional to classical nucleation theory free energy barriers should scale with the quantity $\Delta\mu/\Delta\mu_{\text{spin}}$, the difference in chemical potential between the bulk superheated and the saturated liquid divided by the chemical potential difference between the liquid spinodal and the saturated liquid. The critical bubble changes from classical near coexistence (sharp interface, uniform density that decreases with penetration into the coexistence region) to nonclassical beyond $\Delta\mu/\Delta\mu_{\text{spin}}\approx 0.5$ (diffuse interface, increasing density with increasing penetration into the metastable region). The density at the center of the bubble, the mean bubble density, the bubble size, the interfacial thickness, and the free energy cost of forming a critical bubble all scale with $\Delta\mu/\Delta\mu_{\text{spin}}$ in temperature-independent fashion. This precise measure of the degree of metastability should emerge as a natural parameter in data correlation, as well as in the development of improved theories of nucleation. © *2001 American Institute of Physics.* [DOI: 10.1063/1.1344604]

I. INTRODUCTION

Metastable liquids play crucial roles in a variety of technologically important situations ranging from crystallization and glass formation[1] to cavitation,[2] sonoluminescence,[3] and explosive boiling.[4,5] Despite their ubiquitous presence in nature and technology, major gaps remain in our fundamental understanding of liquids outside their normal range of stability. Prominent among these is the subject of bubble formation in superheated liquids, which remains incompletely understood over a broad range of length scales. From a continuum perspective, the fluid mechanics of bubble formation and collapse remains a topic of active interest, and is key to understanding cavitation erosion and sonoluminescence.[2,6–8] At the microscopic level, it is possible to distinguish between two mechanisms of bubble formation: heterogeneous and homogeneous nucleation. In the former case, dissolved or suspended impurities, or the solid walls of a container can act as preferential sites that facilitate the formation of a microscopic vapor–liquid interface. Heterogeneous nucleation is important in many practical applications, such as boiling heat transfer.[9] In the absence of extraneous surfaces, the liquid–vapor interface must be formed within the bulk superheated liquid itself, by homogeneous nucleation. The work of forming of a new phase is composed of two contributions. The first is the cost of forming an interface, which is proportional to the surface area, and the second is the favorable thermodynamic driving force tending to lower the free energy of the system. The competition between these two contributions gives rise to a critically-sized bubble, beyond which the bubble grows spontaneously into the stable vapor and below which the vapor embryo collapses back into the metastable liquid. The formation of such critically-sized bubbles is the phenomenon of interest here. Knowledge of the energetics, rates, and mechanism of homogeneous bubble nucleation is important for determining attainable limits of liquid superheating,[10] mapping the conditions that lead to industrially hazardous explosive boiling,[11] and preventing catastrophic accidents that can occur during the rapid decompression of tanks containing pressurized liquids.[12] In this paper, we address homogeneous bubble nucleation in an atomic liquid under tension. The low (i.e., substantially subcritical) temperatures involved distinguish this situation from bubble nucleation in near-critical fluids, where other effects, such as the pronounced temperature dependence of the surface tension, become important.

Homogeneous nucleation is one of the basic mechanisms by which first-order phase transitions occur.[1] In general, the rate of nucleation can be written in Arrhenius form,

$$J = A \exp\left(\frac{-W^*}{k_B T}\right), \tag{1}$$

where J is the nucleation rate, that is to say the number of critical nuclei of the stable phase formed per unit time and volume, A is a purely kinetic frequency factor that depends weakly on temperature, k_B is Boltzmann's constant, T is temperature, and W^* is the nucleation free energy barrier, or the reversible work of formation of a critical nucleus. While nucleation is a dynamic process, most theoretical treatments focus on the thermodynamic problem of calculating the free energy barrier height, an approach that finds practical justification in the fact that the nucleation rate has an exponential dependence on this quantity. To estimate the height of the barrier, an underlying construct in most nucleation theories is the physical cluster, that is to say, the embryo of the emerging thermodynamically stable phase. In the so-called classi-

a)Author to whom correspondence should be addressed. Electronic mail: pdebene@princeton.edu

cal nucleation theory[13] (CNT), this embryo is treated as a macroscopic object possessing the properties of the bulk stable phase with a sharp interface separating it from the metastable mother liquor. Despite its limitations, such as its failure to account for any transition from metastability to instability, classical nucleation theory still provides a basic reference with which to compare new theories and interpret experimental measurements.

While the intuitive picture of a physical cluster, that is to say the embryo of the emerging phase, is straightforward to envision, particularly for droplet formation and crystallization, the rigorous identification of such an entity based on the principles of statistical mechanics is nontrivial.[14–16] The problem of identifying a physical cluster is even more complicated for bubble nucleation, the focus of this paper. Umbrella sampling techniques, first employed in the context of nucleation by Frenkel and co-workers to study crystallization,[17] have recently been used to calculate free energy barriers for homogeneous bubble nucleation in superheated liquids.[18,19] In both studies, a global order parameter was used to describe the reaction coordinate. Furthermore, while making no assumptions about the shape of the critical bubble, both studies observed critical nuclei composed largely of cavities, or regions of space devoid of atom centers. In reality, of course, a bubble is more accurately described as a low-density region within the bulk metastable liquid, and identification of such regions within a liquid requires an appropriate microscopic definition of a bubble. However, a local order parameter that can serve as a reaction coordinate in computational studies of bubble nucleation without imposing spherical symmetry to the embryo *a priori* has not been found to date.

Density-functional theory (DFT) approaches to nucleation, pioneered by Oxtoby, e.g.,[20] allow accurate calculations of free energy barriers and critical density profiles by expressing the free energy as a functional of a spatially-varying density. It is implicitly assumed that the system of interest can be coarse-grained, so that one can describe it in terms of a smoothly-varying local density, $\rho(\mathbf{r})$. While most DFT studies have focused on droplet formation and crystallization,[21–31] relatively little attention has been paid to its application to bubble nucleation.[20,24,32,33] In an early DFT study on bubble nucleation, Hooper and Nordholm[33] used generalized van der Waals theory to study the work of formation of and the number of molecules in the critical bubble for the Lennard-Jones fluid. However, for numerical simplicity in the free energy calculations, they assumed the density profile for the critical bubble to be a step function. Oxtoby and co-workers[20,24,32] examined homogeneous bubble nucleation in the Yukawa and Lennard-Jones liquids and He^3 using more sophisticated numerical techniques to locate the critical density profile. These early studies identified nonclassical effects in bubble nucleation for the first time, but calculations were performed only for a limited number of state points. In this paper, we present a systematic study of bubble nucleation in the stretched Lennard-Jones fluid over a broad range of temperatures and tensions, using density-functional theory. The proper scaling of quantities such as the free energy barrier height with respect to the degree of metastability is an important aspect of this work, and we address this question theoretically and numerically. The format of this paper is as follows: In Sec. II we derive theoretical scaling expressions, and we provide a brief description of density-functional theory. The DFT calculations are presented and discussed in Sec. III, and the main conclusions are summarized in Sec. IV.

II. SCALING RELATIONSHIPS AND DENSITY FUNCTIONAL THEORY

A. Barrier height scaling in bubble nucleation

In this subsection, we extend to bubble nucleation the scaling analysis introduced by McGraw and Laaksonen,[34] and subsequently extended by Talanquer.[35] We show that despite the important differences between bubble and droplet nucleation, similar constraints apply in both cases to the relationship between barrier heights, thermodynamic driving force, and size of the critical nucleus.

As noted in Sec. I, the critical nucleus in the CNT is assumed to be macroscopic in size[36] and to have the same thermodynamic properties of the bulk, stable phase. The reversible work of formation of a spherical critical nucleus (free energy barrier) is then given by the expression[1,37,38]

$$W^* = \frac{16\pi\gamma^3}{3(\Delta P)^2}, \tag{2}$$

where γ is the interfacial tension and ΔP is the pressure difference between the interior of the critical nucleus and the bulk mother phase. This expression is valid for bubble as well as for droplet nucleation.[36] The theory works well in the vicinity of phase coexistence, where the critical nucleus and the free energy barrier are large. Near the spinodal, however, the CNT fails badly, as it predicts a finite free energy barrier. This is a direct consequence of the assumption that the critical nucleus is homogeneous.

Using the original form of the nucleation theorem,[39]

$$\frac{dW^*}{d\Delta\mu} = -n^*, \tag{3}$$

McGraw and Laaksonen[34] introduced useful scaling relations for homogeneous droplet nucleation. These are given as

$$n^* = C(T)\cdot(\Delta\mu)^{-3} \tag{4}$$

and

$$W^* = \tfrac{1}{2}\cdot n^*\cdot\Delta\mu - D(T). \tag{5}$$

In Eqs. (3)–(5), W^* is the work of formation of a critical nucleus, $\Delta\mu$ is the chemical potential difference between the supersaturated and saturated vapor, and n^* is the number of molecules in the critical droplet. $C(T)$ and $D(T)$ are temperature-dependent constants that quantify the deviation from classical behavior. Koga and Zeng[40] performed a series expansion of the classical work of nucleation in powers of $\Delta\mu$ about coexistence, where the coefficients can be calculated from bulk properties. They showed that the McGraw–Laaksonen scaling relations are a limiting case of their series expansion, that is to say Eqs. (4) and (5) can be obtained by setting higher order terms to zero. Shortly after the introduc-

tion of the scaling relations, Talanquer[35] obtained expressions for constants $C(T)$ and $D(T)$ by using the fact that the free energy barrier vanishes at the spinodal. Furthermore, he was able show that, within the approximations involved in the McGraw–Laaksonen treatment[34] (to be discussed below), the height of the free energy barrier should be a quadratic function of $\Delta\mu$,

$$\frac{W^*}{\frac{1}{2}\cdot n^*\cdot\Delta\mu}=1-\left(\frac{\Delta\mu}{\Delta\mu_{\text{spin}}}\right)^2, \tag{6}$$

where $\Delta\mu_{\text{spin}}$ is the chemical potential difference between the binodal and vapor spinodal at the same temperature. Noting that in the CNT, the quantity $n^*\Delta\mu/2$ is the work of formation, W^*_{CNT}, Eq. (6) says that the ratio of the actual work of droplet formation to the classical work should be a simple quadratic function of $\Delta\mu/\Delta\mu_{\text{spin}}$.

Although the McGraw–Laaksonen and Talanquer scaling relations were derived specifically for the case of droplet formation, we show that similar relationships exist for bubble nucleation. We begin by writing the nucleation theorem in a more general form, as derived by Oxtoby and Kashchiev,[41]

$$\frac{dW^*}{d\Delta\mu}=-\Delta n^*, \tag{7}$$

where Δn^* (<0 for bubble nucleation) is the *excess* number of molecules in the critical nucleus with respect to the number of molecules in the metastable mother phase in the same volume, and $\Delta\mu$ (<0) is the chemical potential difference between the metastable and saturated *mother phase* at the given temperature. It should be noted that the derivative in Eq. (7) is taken at constant temperature. Next, the classical work of bubble formation, W^*_{CNT},[36,37] is written as

$$W^*_{\text{CNT}}=\frac{16\pi\gamma^3}{3(P^*-P)^2}, \tag{8}$$

where P^* is the pressure within the critical nucleus and P is the bulk pressure in the superheated liquid. For a sufficiently large spherical embryo, the excess number of molecules in the critical bubble, Δn^*, is

$$\Delta n^*=\frac{-32\pi\gamma^3}{3(P^*-P)^3}\rho_L, \tag{9}$$

where ρ_L is the number density of the metastable liquid. Equation (9) is valid under the assumption that the density of the superheated liquid is much larger than that of the vapor in the critical bubble. This is an excellent approximation for modest superheating and away from the critical point. At sufficiently subcritical temperatures, and for modest superheating, the bulk metastable liquid can be considered incompressible. The chemical potential difference between the superheated and the saturated liquid at the same temperature is then given by

$$\Delta\mu=\frac{1}{\rho_L}(P-P_{\text{sat}}), \tag{10}$$

where P_{sat} is the vapor pressure at the given temperature. Combining Eqs. (8), (9), and (10) and using the fact[1] that $P^*\to P_{\text{sat}}$ as $\Delta\mu\to 0$, where classical theory is known to work, it follows that

$$\frac{W^*_{\text{CNT}}}{\Delta\mu\cdot\Delta n^*}=\frac{1}{2}. \tag{11}$$

Thus, in the limit where the classical picture applies, namely modest superheating and away from criticality, we recover the same expression for the barrier height in terms of supersaturation and size of the critical nucleus as was found for droplet nucleation.

Following the approach of McGraw and Laaksonen,[34] it is postulated that the ratio of the nonclassical work of nucleation, W^*, to the quantity $\Delta\mu\cdot\Delta n^*$ can be written in the general form,

$$\frac{W^*}{\Delta\mu\cdot\Delta n^*}=\frac{1}{2}-f(\Delta n^*,\Delta\mu), \tag{12}$$

where the function $f(\Delta n^*,\Delta\mu)$ describes the departure from classical behavior. Differentiating Eq. (12) with respect to $\Delta\mu$ at constant temperature and using the nucleation theorem, Eq. (7), yields the following differential equation that could in theory be solved, provided that $f(\Delta n^*,\Delta\mu)$ is known:

$$3\Delta n^*+\Delta\mu\cdot\frac{d}{d\Delta\mu}\Delta n^*=2\frac{d}{d\Delta\mu}[\Delta\mu\cdot\Delta n^*\cdot f(\Delta n^*,\Delta\mu)]. \tag{13}$$

Since $f(\Delta n^*,\Delta\mu)$ is not known in general, McGraw and Laaksonen[34] assumed that both sides of Eq. (13) vanish identically, and each side can be solved separately to yield solutions for Δn^* and $f(\Delta n^*,\Delta\mu)$,

$$\Delta n^*=C(T)\cdot(\Delta\mu)^{-3} \tag{14}$$

and

$$\Delta n^*\cdot f(\Delta n^*,\Delta\mu)=D(T)\cdot(\Delta\mu)^{-1}, \tag{15}$$

where $C(T)$ and $D(T)$ are temperature-dependent constants of integration. $C(T)$ can be deduced from Eqs. (9) and (10). Substituting Eqs. (14) and (15) into Eq. (12) and rearranging, one obtains an expression that relates the difference between the real and classical free energy barriers,

$$W^*=\tfrac{1}{2}\cdot\Delta\mu\cdot\Delta n^*-D(T). \tag{16}$$

In other words, the discrepancy between the classical and actual free energy barrier is solely a function of temperature. Following Talanquer's reasoning,[35] the temperature-dependent constant, $D(T)$, can be obtained by using the fact that the real free energy barrier vanishes at the spinodal,

$$D(T)=\tfrac{1}{2}\cdot C(T)\cdot(\Delta\mu_{\text{spin}})^{-2}, \tag{17}$$

where $\Delta\mu_{\text{spin}}$ (<0) is the chemical potential difference between the liquid spinodal and binodal at the same temperature. Equation (16) can now be rewritten as

$$\frac{W^*}{\Delta\mu\cdot\Delta n^*}=\frac{1}{2}\cdot\left[1-\left(\frac{\Delta\mu}{\Delta\mu_{\text{spin}}}\right)^2\right] \tag{18}$$

which is almost identical to Talanquer's scaling relation for droplet formation, Eq. (6), except that we have used the excess number of molecules, Δn^*, rather than the actual number in the critical nucleus, n^*. This distinction is important in bubble nucleation, but not in droplet nucleation. Equation (18) is therefore a scaling relation that holds for both droplet and bubble nucleation, even though the mechanisms driving the two phase transitions are quite different. The significance of Eq. (18) transcends the specific functional form, the accuracy of which will be investigated in Sec. III through DFT. More importantly, this equation points to the ratio $\Delta\mu/\Delta\mu_{\text{spin}}$ as a natural measure of the degree of metastability. It will be shown in Sec. III that the free energy barrier to nucleation, as well as the mean density, size, and interfacial thickness of the critical bubble all scale with $\Delta\mu/\Delta\mu_{\text{spin}}$ in a temperature-independent fashion.

B. Density-functional theory

The density functional approach to nucleation was first implemented by Oxtoby and Evans[20] in a study of droplet formation in the Yukawa fluid and has since been used to study nucleation in other systems.[24,27–32] A detailed discussion of the theory can be found in Oxtoby.[42] Here, we simply summarize key aspects of DFT.

In density-functional theory, it is assumed that the free energy is a functional of a smoothly-varying spatial density, $\rho(\mathbf{r})$. The interactions between atoms are normally taken to be pairwise additive, with the pair potential consisting of a hard-core repulsion and a weak attractive tail. The pair potential, $\phi(r)$, can then be written as

$$\phi(r)=\phi_{\text{ref}}(r)+\phi_{\text{pert}}(r), \tag{19}$$

where $\phi_{\text{ref}}(r)$ represents the steep, repulsive portion of the potential, and $\phi_{\text{pert}}(r)$ represents the weak attractive part. In this regard, ϕ_{ref} serves as a reference system potential and ϕ_{pert} serves as a slight perturbation. For pairwise additive systems, the functional derivative of the Helmholtz free energy with respect to the pair potential is proportional to the pair distribution function $\rho^{(2)}(\mathbf{r},\mathbf{r}')$,

$$\frac{\delta F}{\delta\phi(\mathbf{r},\mathbf{r}')}=\frac{1}{2}\rho^{(2)}(\mathbf{r},\mathbf{r}'). \tag{20}$$

Functional integration leads directly to the Helmholtz free energy,

$$F[\rho]=F_{\text{ref}}[\rho]+\frac{1}{2}\int_0^1 d\alpha\int\int d\mathbf{r}\,d\mathbf{r}'\,\rho^{(2)}(\mathbf{r},\mathbf{r}';\phi_\alpha)\times\phi_{\text{pert}}(\mathbf{r},\mathbf{r}'), \tag{21}$$

where a linear integration path over α is chosen for convenience, since the free energy functional must be independent of the integration path chosen. The simplest approximation for the pair distribution function is the random phase approximation (RPA), in which all particle–particle correlations are ignored,

$$\rho^{(2)}(\mathbf{r},\mathbf{r}')\approx\rho(\mathbf{r})\rho(\mathbf{r}'). \tag{22}$$

Specifically, the radial distribution function, $g(r)$, is assumed to be unity. While more sophisticated approximations exist, the RPA has been shown to be quantitatively accurate for systems with weak inhomogeneities like the liquid–vapor interface.[43]

The reference state included in Eqs. (19) and (21) is usually taken to be an equivalent hard sphere system, and its Helmholtz free energy can be written in the general form,

$$F_{\text{ref}}[\rho]=\int d\mathbf{r}\,f_{\text{hs}}(\rho(\mathbf{r})), \tag{23}$$

where $f_{\text{hs}}(\rho)$ is the hard sphere Helmholtz free energy per unit volume at a density ρ. This can be calculated easily from an equation of state, for example, the Carnahan–Starling[44] hard sphere equation of state,

$$P_{\text{hs}}(\rho)=\frac{k_BT(1+\eta+\eta^2-\eta^3)}{(1-\eta)^3}, \tag{24}$$

where η, the packing fraction, is $(\pi/6)\rho d^3$ and d is the hard sphere diameter.

To model the Lennard-Jones (LJ) system using density-functional theory, we follow the approach used by Zeng and Oxtoby[24] in their nucleation studies of the same system, where the potential is broken up using the Weeks, Chandler, and Anderson (WCA) (Ref. 45) perturbation scheme. The Lennard-Jones interaction potential between a pair of atoms is given by

$$\phi_{\text{LJ}}(r)=4\epsilon\left[\left(\frac{\sigma}{r}\right)^{12}-\left(\frac{\sigma}{r}\right)^{6}\right], \tag{25}$$

where ϵ is the value of the potential energy minimum and σ is the interatomic separation where the potential energy is zero. In the WCA perturbation scheme, the potential is divided into its repulsive and attractive parts, $\phi_1^{\text{WCA}}(r)$ and $\phi_2^{\text{WCA}}(r)$, respectively,

$$\phi_1^{\text{WCA}}(r)=\begin{cases}\phi_{\text{LJ}}(r)+\epsilon & r<r_{\min}\\ 0 & r\geqslant r_{\min}\end{cases}, \tag{26}$$

$$\phi_2^{\text{WCA}}(r)=\begin{cases}-\epsilon & r<r_{\min}\\ \phi_{\text{LJ}}(r) & r\geqslant r_{\min}\end{cases}, \tag{27}$$

where $r_{\min}$ is $2^{1/6}\sigma$, the location of the potential energy minimum. The repulsive part, $\phi_1^{\text{WCA}}(r)$, is mapped onto an equivalent hard sphere system following the scheme put forth by Lu *et al.*,[46] using a temperature-dependent hard sphere diameter

$$d(T)=\frac{a_1T+b}{a_2T+a_3}\cdot\sigma, \tag{28}$$

where $a_1=0.561\,65k_B/\epsilon$, $a_2=0.608\,99k_B/\epsilon$, $a_3=0.928\,68$, and $b=0.9718$. ϕ_2^{WCA} now serves as the perturbation potential for this equivalent hard sphere system.

Since the grand potential is related to the Helmholtz free energy by

$$\Omega[\rho]=F[\rho]-\mu\int d\mathbf{r}\,\rho(\mathbf{r}), \tag{29}$$

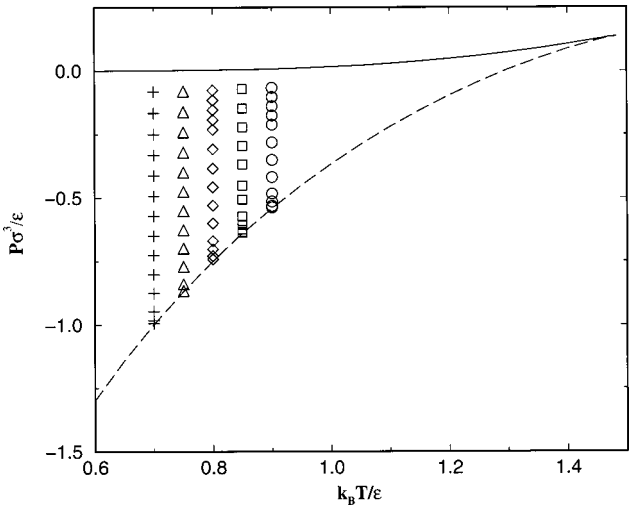

FIG. 1. Liquid–vapor phase diagram for the Lennard-Jones fluid in the $P-T$ plane. The solid line is the binodal, and the dashed line is the liquid spinodal. The calculations were performed at state points along isotherms, k_BT/ϵ, of 0.70 (+), 0.75 (△), 0.80 (◇), 0.85 (□), and 0.90 (○).

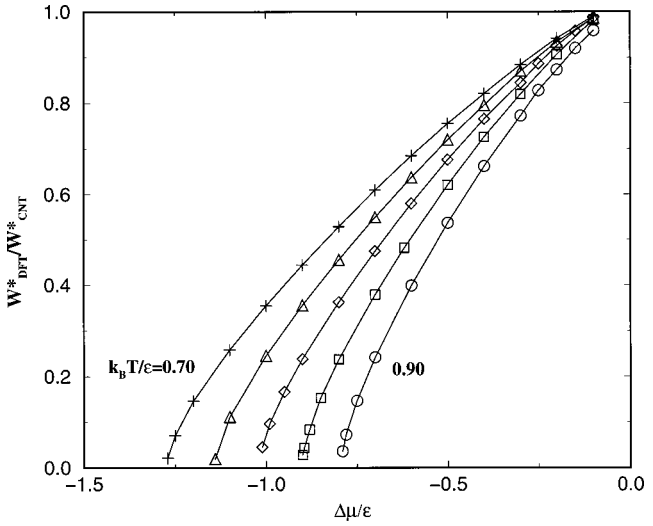

FIG. 2. Ratio of density functional to classical free energy barriers, $W^*_{\mathrm{DFT}}/W^*_{\mathrm{CNT}}$, plotted against the chemical potential difference, $\Delta\mu/\epsilon$, between the bulk metastable liquid and the saturated liquid at the same temperature. Calculations were performed at reduced temperatures k_BT/ϵ of 0.70 (+), 0.75 (△), 0.80 (◇), 0.85 (□), and 0.90 (○).

where μ is the chemical potential, the grand potential of the system can now be written as

$$\Omega[\rho]=\int d\mathbf{r}\, f_{\mathrm{hs}}(\rho(\mathbf{r}))-\mu\int d\mathbf{r}\,\rho(\mathbf{r}) + \frac{1}{2}\int\int d\mathbf{r}\,d\mathbf{r}'\,\rho(\mathbf{r})\rho(\mathbf{r}')\phi_2^{\mathrm{WCA}}(\mathbf{r},\mathbf{r}'). \tag{30}$$

The density profile of the critical nucleus and the free energy barrier can be found by solving the following integral equation,

$$\mu_{\mathrm{hs}}(\rho(\mathbf{r}))=\mu-\int d\mathbf{r}'\,\phi_2^{\mathrm{WCA}}(\mathbf{r},\mathbf{r}')\rho(\mathbf{r}'), \tag{31}$$

which is obtained by setting the functional derivative of the grand potential with respect to density equal to zero, $\delta\Omega[\rho]/\delta\rho(\mathbf{r})=0$. The solution of this equation relevant to nucleation, a saddle point in functional space, is unstable when the chemical potential is not that corresponding to phase coexistence, and thus standard iterative methods will not naturally converge. The numerical method for locating the critical profile is described in detail in Refs. 20 and 24. For simplicity, spherical symmetry is assumed to exist, reducing Eq. (31) to a one-dimensional integral equation.

III. RESULTS AND DISCUSSION

Density profiles and the corresponding free energy barriers for the critical bubble were calculated at five different temperatures ($k_BT/\epsilon=0.70$, 0.75, 0.80, 0.85, and 0.90) for a range of chemical potentials that placed the liquid under tensions, $P\sigma^3/\epsilon$, ranging from -0.067 to -0.99 (Fig. 1). These calculations were performed by fixing the bulk (metastable) chemical potential and temperature, and varying the uniform density [i.e., using Eq. (30) with uniform ρ and fixed μ]. In general, this procedure yields two minima for Ω/V as a function of ρ. One corresponds to the metastable liquid (results shown in Fig. 1) and the other to the stable vapor having the same chemical potential. For a uniform fluid, $\Omega=-PV$, which allows the calculation of the pressure.

Comparisons to the classical free energy barrier were made using Eq. (2), with γ obtained from the planar surface tension calculations of Zeng and Oxtoby[24] for the same system. Figure 2 shows the ratio of density-functional (DFT) to classical (CNT) free energy barriers, $W^*_{\mathrm{DFT}}/W^*_{\mathrm{CNT}}$, as a function of the chemical potential difference, $\Delta\mu$ (<0),

$$\Delta\mu=\mu_{\mathrm{liq}}-\mu_{\mathrm{sat}}(T), \tag{32}$$

where $\mu_{\mathrm{sat}}(T)$ is the coexistence chemical potential at the specified temperature, T, and μ_{liq} is the chemical potential of the bulk metastable liquid. As noted above, μ_{liq} and T are inputs to a homogeneous DFT calculation. Minimization of the grand potential (per unit volume) with respect to density yields two solutions for phases of uniform density, corresponding to the stable vapor (V) and the metastable liquid (L) (Fig. 3). Note that both μ and T are fixed in this calculation, and ρ is therefore an order parameter with respect to

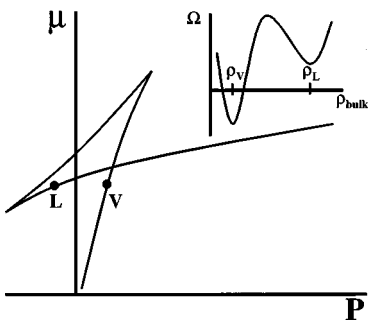

FIG. 3. Schematic metastable liquid and stable vapor states in $\mu-P$ and $\Omega-\rho$ planes at constant temperature. The chemical potential corresponding to the metastable liquid (L) and stable vapor (V) is an input to the inhomogeneous density-functional calculation.

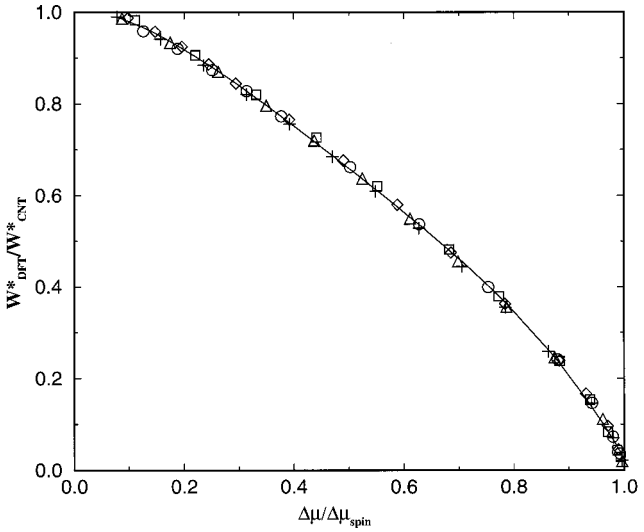

FIG. 4. Ratio of density functional to classical free energy barriers, $W^*_{\mathrm{DFT}}/W^*_{\mathrm{CNT}}$, plotted against the degree of metastability, $\Delta\mu/\Delta\mu_{\mathrm{spin}}$, where $\Delta\mu_{\mathrm{spin}}=\mu_{\mathrm{spin}}(T)-\mu_{\mathrm{sat}}(T)$. μ_{spin} is the chemical potential at the liquid spinodal, corresponding to the limit of stability of the superheated liquid at temperature T. The line is a guide to the eye. Calculations were performed at reduced temperatures k_BT/ϵ of 0.70 (+), 0.75 (△), 0.80 (◇), 0.85 (□), and 0.90 (○).

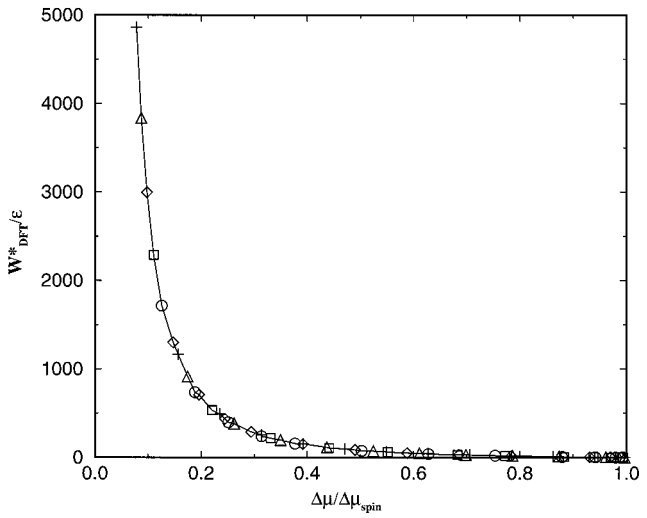

FIG. 5. Density-functional theory prediction for the free energy barrier height, W^*_{DFT}, plotted against the degree of metastability, $\Delta\mu/\Delta\mu_{\mathrm{spin}}$. The solid curve is a guide to the eye. Temperature symbols are the same as in Fig. 1.

which the free energy is minimized, rather than an independent thermodynamic variable. The density of the metastable liquid is an input to the inhomogeneous DFT calculation, since it ''pins'' one end of the density profile of the critical bubble to the bulk metastable phase. As expected near coexistence, the ratio of free energy barriers is very close to unity; away from coexistence, the deviation between the two theories increases. It is important to note that W^*_{DFT} correctly vanishes at the spinodal, whereas W^*_{CNT} remains positive.

In order to quantify the degree of metastability of the stretched liquid, it is convenient to scale $\Delta\mu$ by the difference in chemical potentials between the liquid spinodal and the binodal at the same temperature, $\Delta\mu_{\mathrm{spin}}(<0)$,

$$\Delta\mu_{\mathrm{spin}}=\mu_{\mathrm{spin}}(T)-\mu_{\mathrm{sat}}(T). \tag{33}$$

The ratio $\Delta\mu/\Delta\mu_{\mathrm{spin}}$ yields a measure of metastability that ranges from zero at coexistence to unity at the spinodal. Figure 4 shows the ratio of DFT and CNT free energy barriers as a function of the degree of metastability, $\Delta\mu/\Delta\mu_{\mathrm{spin}}$, at the same five temperatures of Fig. 2. Note, as in Fig. 2, the limiting behavior near coexistence ($W^*_{\mathrm{DFT}}/W^*_{\mathrm{CNT}}\to 1$ as $\Delta\mu/\Delta\mu_{\mathrm{spin}}\to 0$) and near the spinodal ($W^*_{\mathrm{DFT}}/W^*_{\mathrm{CNT}}\to 0$ as $\Delta\mu/\Delta\mu_{\mathrm{spin}}\to 1$). The striking feature of this plot is that all the free energy barriers now collapse onto the same curve, indicating that the deviations from the classical barrier height are predicted by density-functional theory to be solely a function of the scaled degree of penetration into the metastable region. In Fig. 5, the free energy barrier height, as predicted by DFT, is plotted against the degree of metastability. It can be seen that the work of forming a critical bubble does not depend explicitly on temperature, but is instead only a function of $\Delta\mu/\Delta\mu_{\mathrm{spin}}$. The scaling of W^*_{DFT} with $\Delta\mu/\Delta\mu_{\mathrm{spin}}$ is a result that is not obvious *a priori* neither in the classical nor density-functional formulation of nucleation.

Figure 6 shows the DFT-calculated density profile for the critical bubble near coexistence ($\Delta\mu/\epsilon=-0.1$ or $\Delta\mu/\Delta\mu_{\mathrm{spin}}=0.078$) at $k_BT/\epsilon=0.70$. The density at the center of the bubble is very close to that of the stable vapor and is uniform up to the interface. Note that the interface is sharp on the length scale of the bubble radius, and this agrees well with the classical picture. In contrast, the critical density profile near the liquid's limit of stability ($\Delta\mu/\epsilon=-1.25$ or $\Delta\mu/\Delta\mu_{\mathrm{spin}}=0.98$) at the same temperature is shown in Fig. 7. The critical bubble is now very different from the classical prediction; there is no sharp interface between the bubble and the metastable liquid. Furthermore, the vapor, even at

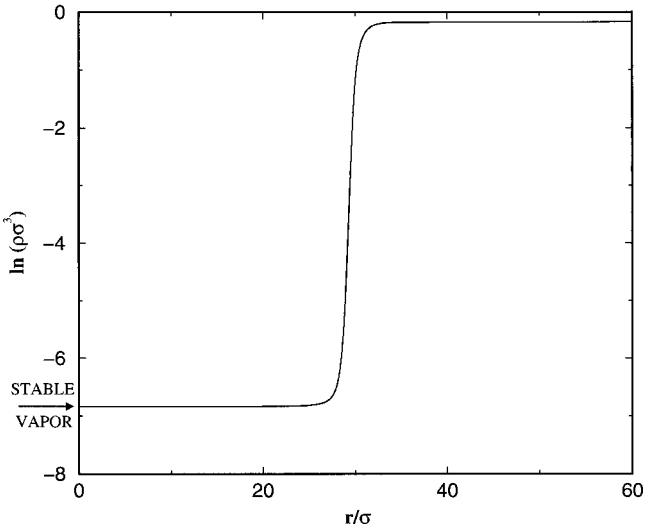

FIG. 6. Density profile for the critical bubble near coexistence ($\Delta\mu/\epsilon=-0.1$ or $\Delta\mu/\Delta\mu_{\mathrm{spin}}=0.078$) at $k_BT/\epsilon=0.70$. The density of the stable vapor is marked for comparison with the classical theory prediction.

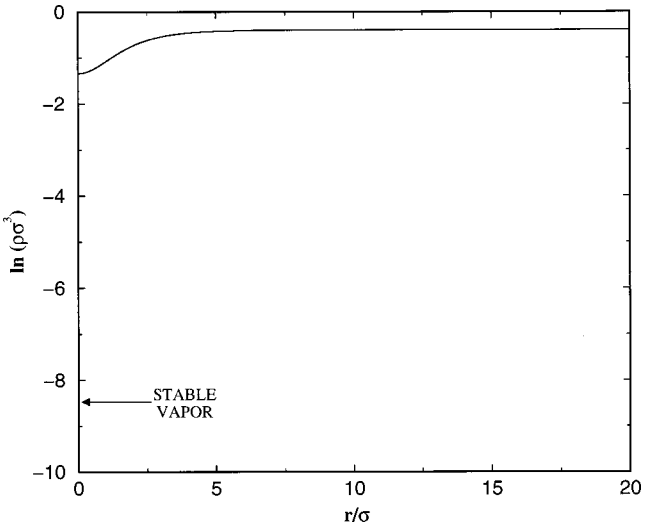

FIG. 7. Density profile for the critical bubble near the limit of stability ($\Delta\mu/\epsilon=-1.25$ or $\Delta\mu/\Delta\mu_{\rm spin}=0.98$) at $k_BT/\epsilon=0.70$. The density of the stable vapor is indicated for comparison with the classical theory prediction.

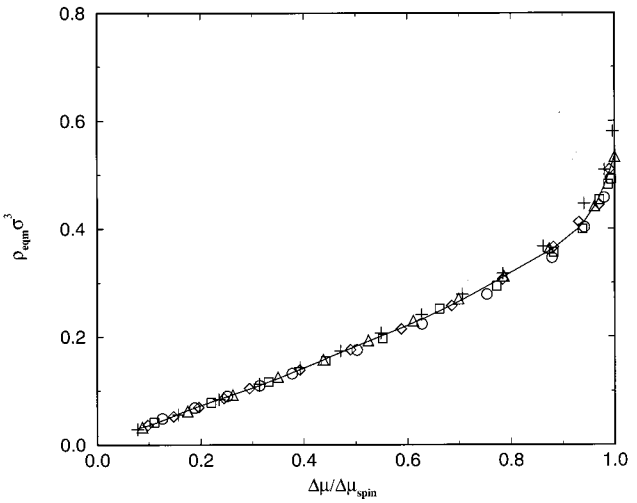

FIG. 9. Mean bubble density calculated using the radial position of the equimolar dividing surface as a function of metastability, $\Delta\mu/\Delta\mu_{\rm spin}$, at various temperatures. The line is a guide to the eye. Temperature symbols are the same as in Fig. 1.

the center of the bubble, is much denser than the stable vapor. Figure 8 shows how the density at the center of the bubble changes as a function of the degree of metastability at different temperatures. Upon entering the metastable region, the density at the center at first decreases, since the density of the vapor having the same chemical potential as the stretched liquid decreases as $|\Delta\mu|$ increases. This can be described as a bulk thermodynamic effect. However, upon approaching the spinodal, the density at the center increases, becoming almost liquidlike. This is consistent with the fact that, as the mechanism responsible for the phase transition changes from nucleation to spinodal decomposition, the relevant density fluctuations in turn change from small wavelength, large amplitude (i.e., a vaporlike critical nucleus) to long-wavelength fluctuations of arbitrary amplitude. The combination of these two effects gives rise to a minimum in the density at the center of the critical bubble as a function of degree of metastability. We note that this minimum occurs at $\Delta\mu/\Delta\mu_{\rm spin}=0.5\pm0.005$ over the range of temperatures studied here.

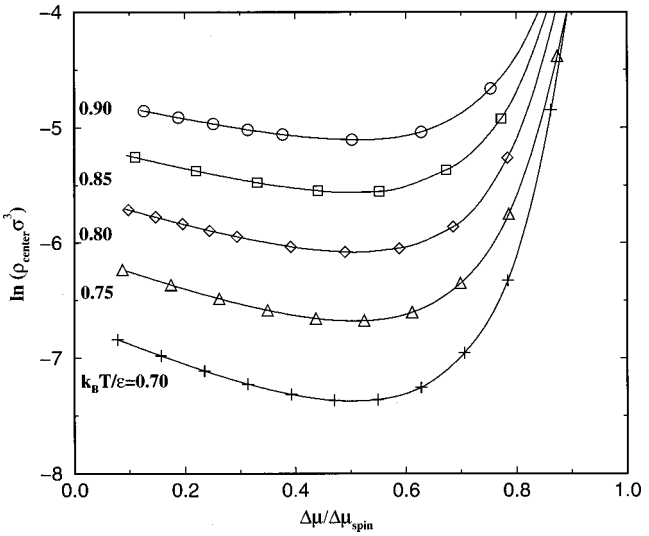

FIG. 8. Dependence of the density at the center of the critical bubble on the degree of metastability. The minimum in density occurs at $\Delta\mu/\Delta\mu_{\rm spin}=0.5\pm0.005$ for all temperatures.

It is interesting to examine the evolution of the mean density as the extent of penetration into the coexistence region increases. In this work, we determine the mean density by integrating the density profile from the origin to the radial position of the equimolar dividing surface, whose location is defined such that there is no surface adsorption, or excess, when the true liquid density profile is imagined replaced by the bulk liquid density up to the dividing surface and, likewise, the true bubble density profile is imagined replaced by the density at the center up to the dividing surface.[47] We denote the mean density calculated in this manner by $\rho_{\rm eqm}$ and the radial position of the surface by $R_{\rm eqm}$. The mean density using the equimolar dividing surface is plotted against the degree of metastability at various temperatures in Fig. 9. Note that the average density of the critical bubble increases with penetration into the metastable region, contrary to classical expectations. In the classical picture, the critical nucleus is assumed to have the uniform density of the stable vapor at the same chemical potential, and thus the average critical bubble density is expected to decrease with increasing metastability. A remarkable feature of this plot is that up to appreciable degrees of metastability, the mean density calculated using the equimolar surface collapses onto a single curve, independent of temperature. Note that the scaling of the mean density breaks down close to the spinodal, where density fluctuations become arbitrarily large. Similar temperature-independent behavior is also observed when the surface of tension is used to calculate the mean density.

The equimolar dividing surface also serves as a convenient means to define the size of the critical nucleus, whose radius is given simply by the radial position of the surface, $R_{\rm eqm}$. In Fig. 10 we plot this definition of nucleus size versus the degree of metastability at the five temperatures studied.

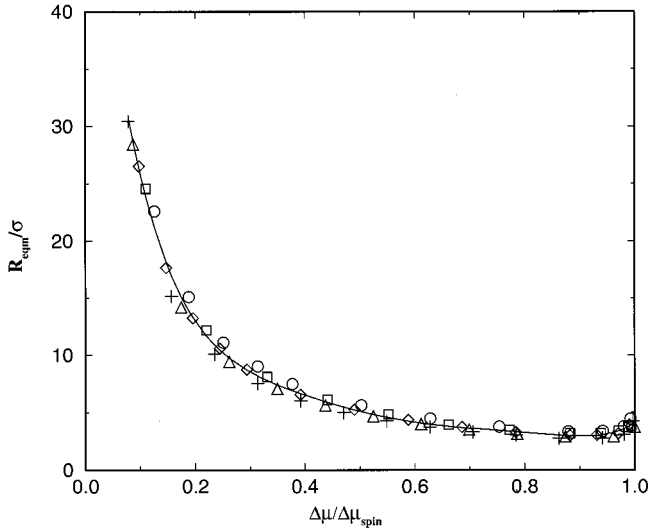

FIG. 10. Radial location of the equimolar dividing surface for the critical bubble as a function of metastability, $\Delta\mu/\Delta\mu_{\text{spin}}$, at various temperatures. The line is a guide to the eye. Temperature symbols are the same as in Fig. 1.

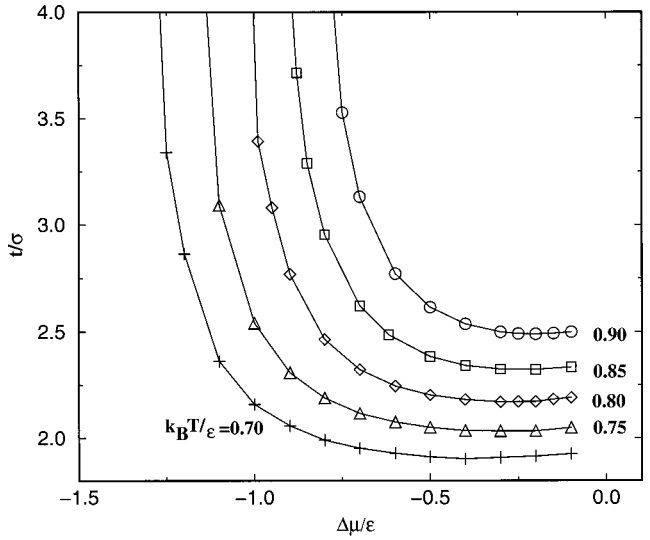

FIG. 11. Interfacial thickness of the critical bubble as a function of $\Delta\mu/\epsilon$ at various temperatures.

In all cases, the radius of the critical nucleus initially decreases with the degree of metastability, which is consistent with thermodynamic expectations. While the data points do not fall perfectly onto the same curve, the size of the critical nucleus is, to an excellent approximation, a function of the degree of metastability, independent of temperature, over the temperature range investigated here. Note that close enough to the spinodal, the size of the critical bubble reaches a minimum and then begins to increase with the degree of metastability. This effect, which cannot be predicted by the classical theory, reflects the growth of the interface thickness (see Figs. 6 and 7), which we quantify below. Finally, we mention in passing that the same qualitative behavior, in particular the apparent collapse of data onto a single curve, is observed if the radius of the critical bubble is taken to coincide with the radial position of the surface of tension.

Interfacial widths of the critical bubble were calculated using a 10%–90% criterion, according to which the thickness of the interface is the distance over which the density changes from $[\rho_{\text{center}}+0.1(\rho_{\text{liq}}-\rho_{\text{center}})]$ to $[\rho_{\text{center}}+0.9(\rho_{\text{liq}}-\rho_{\text{center}})]$, where ρ_{center} and ρ_{liq} denote the density at the center of the bubble and in the bulk mother phase, respectively. Figure 11 shows the thickness of the interface, t, as a function of $\Delta\mu$ at different temperatures. As expected, the thickness increases as the liquid spinodal is approached. Furthermore, the interfacial thickness increases with temperature, reflecting the fact that at the critical point there is no distinction between liquid and vapor. Interestingly, at fixed temperature, the width of the interface remains relatively constant over a significant $\Delta\mu$ range before increasing sharply as the spinodal is approached. Figure 12 shows the same data as in Fig. 11, but scaled in such a way that all the curves collapse into one. The normalization factor for t is the minimum interfacial thickness at the given temperature, $t_{\min}$. It can be seen that that the normalized interfacial width remains constant over an appreciable range of metastability, but grows rapidly beyond $\Delta\mu/\Delta\mu_{\text{spin}}=0.5$. We note that this condition is also where the minimum in the density at the center of the critical bubble occurs (Fig. 8).

The ratio of DFT to CNT free energy barriers is described solely by the degree of metastability (Fig. 4). In Sec. II A, we showed that the ratio of free energy barriers should be a quadratic function of metastability for both bubble and droplet nucleation, provided that the same homogeneity assumption is made for bubble nucleation as was made in the original treatment for droplet nucleation.[34] It is interesting to see how the DFT calculation compares with Eq. (18). In Fig. 13, we plot $W^*_{\text{DFT}}/W^*_{\text{CNT}}$ vs $(\Delta\mu/\Delta\mu_{\text{spin}})^2$ alongside the behavior predicted by Eq. (18), where W^*_{CNT} is calculated using Eq. (3). The agreement is only qualitative. The denominator of Eq. (18), $\Delta\mu\Delta n^*/2$, becomes equal to W^*_{CNT} only near

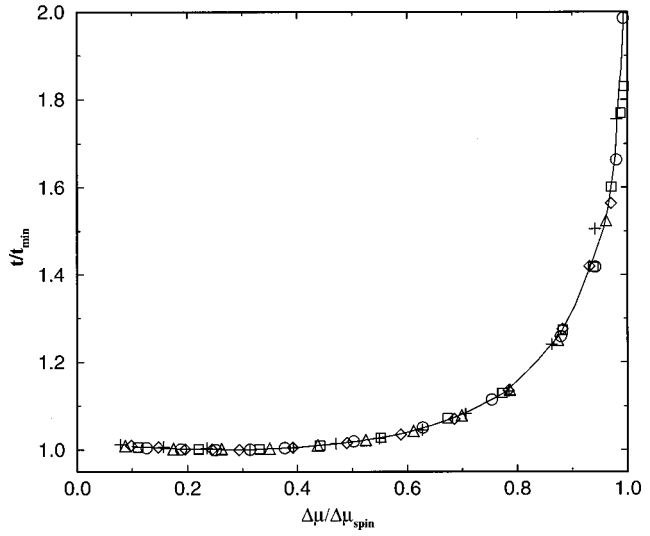

FIG. 12. Normalized interfacial thickness plotted against the degree of metastability. The width of the interface was scaled by the minimum width at each temperature. The line is a guide to the eye. Symbols for each temperature are the same as in Fig. 1.

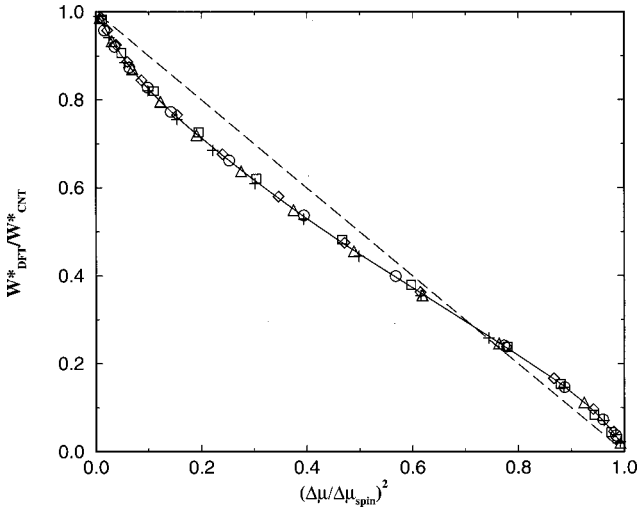

FIG. 13. $W^*_{\mathrm{DFT}}/W^*_{\mathrm{CNT}}$ vs $(\Delta\mu/\Delta\mu_{\mathrm{spin}})^2$. The line through the points is a guide to the eye. The dashed line is the prediction of Eq. (18). Temperature symbols are the same as in Fig. 1.

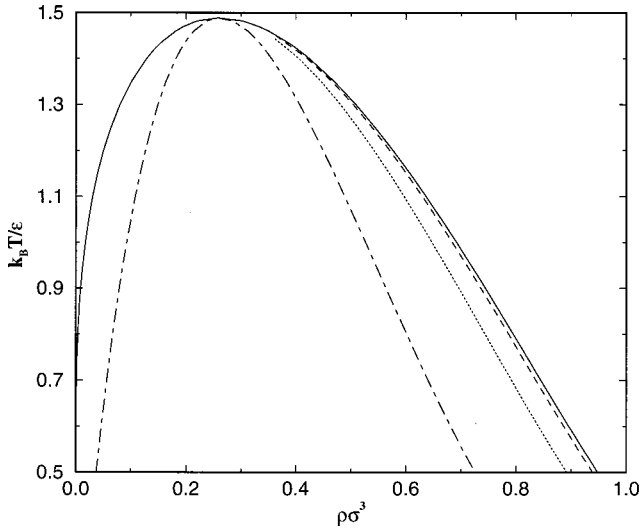

FIG. 15. $T-\rho$ projection of the liquid–vapor phase diagram for the Lennard-Jones model used in this study. The loci $\Delta\mu/\Delta\mu_{\mathrm{spin}}=0.1$ (– – –) and 0.5 (---) are shown, as is the liquid spinodal (–·–).

coexistence. For moderate degrees of superheating, the pressure at the center of the critical bubble can deviate substantially from the equilibrium vapor pressure [see Eqs. (8)–(10)], and hence $W^*_{\mathrm{CNT}} \neq \Delta\mu\Delta n^*/2$. In Fig. 14, we plot the quantity $W^*_{\mathrm{DFT}}/(\Delta\mu\Delta n^*/2)$ vs $(\Delta\mu/\Delta\mu_{\mathrm{spin}})^2$ alongside the prediction of Eq. (18), where Δn^* is calculated from the actual density profile of the critical nucleus and $\Delta\mu$ is the externally imposed chemical potential driving force with respect to coexistence. Plotting the data in this way provides a direct evaluation of Eq. (18). The agreement between the DFT calculations and the predicted scaling is quite good up to $\Delta\mu/\Delta\mu_{\mathrm{spin}} \approx 0.5$, beyond which there are appreciable differences. The quadratic form clearly does not capture DFT behavior completely. This is due to the imposition of the requirement that both sides of Eq. (13) vanish, a key step in deriving Eq. (18). McGraw and Laaksonen[34] have shown that this assumption leads to predictions that agree with DFT calculations for droplet nucleation. Although the vanishing of both sides of Eq. (13) is a reasonable assumption in light of the fact that $f(\Delta n^*, \Delta\mu)$ is unknown, and, furthermore, it allows for the recovery of classical behavior, it is not a rigorous requirement. It remains to be studied how the derivation presented in Sec. II A is affected by assuming *a priori* other reasonable functional forms of $f(\Delta n^*, \Delta\mu)$, that is to say what type of functional form is necessary to describe the deviations from classical behavior shown in Figs. 13 and 14.

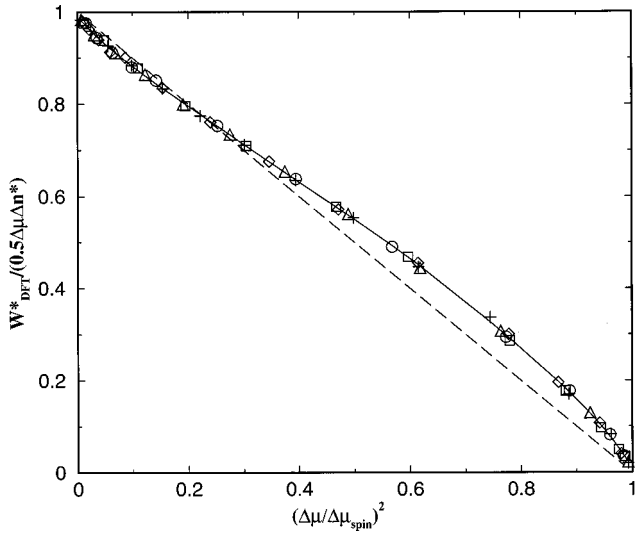

FIG. 14. Direct comparison of the prediction of Eq. (18) (dashed line) with density functional theory. The line through the points is a guide to the eye. Temperature symbols are the same as in Fig. 1.

The various calculated quantities, when plotted against the degree of metastability, $\Delta\mu/\Delta\mu_{\mathrm{spin}}$, exhibit a common feature, namely the competition between binodal and spinodal-dominated behavior. In the vicinity of the binodal, $\Delta\mu/\Delta\mu_{\mathrm{spin}} \to 0$, the assumptions of the classical theory are valid. It is here that the critical nucleus is a large, well-defined geometric object with an internal density practically equal to that of the stable vapor (Fig. 6). Furthermore, in this region, the work of forming such a bubble is given accurately by the classical theory, Eq. (3). At the other extreme, near the spinodal, $\Delta\mu/\Delta\mu_{\mathrm{spin}} \to 1$, the assumptions of the classical theory become increasingly inaccurate, reflecting the gradual change in the phase transition mechanism from nucleation to spinodal decomposition. This latter mechanism is characterized by small amplitude, long-wavelength fluctuations, which within the confines of DFT, results in a critical bubble that is small, diffuse, and liquidlike (Fig. 7). Energetically, the formation of such entities requires little work, since the necessary fluctuations occur almost spontaneously (Fig. 5). Between the binodal and liquid spinodal, there is a smooth transition in terms of the energetics, size, and density of the critical bubble that reflects a competition between binodal and spinodal-dominated behavior. This is exemplified by the behavior of the density at the center of the bubble (Fig. 8), which initially decreases (classical behavior), but then increases upon further penetration into the metastable region, reflecting the fact that the density fluctuations necessary to form a critical nucleus become smaller in magnitude.

Figures 15 and 16 show the loci of points in the (T,ρ)

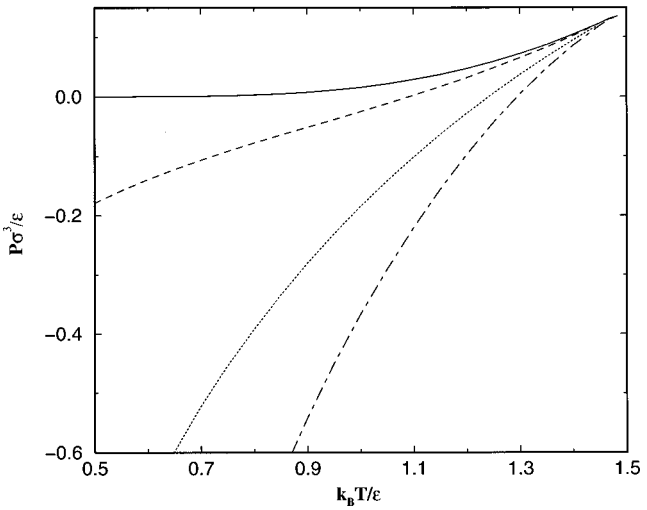

FIG. 16. $P-T$ projection of the liquid–vapor phase diagram for the Lennard-Jones model used in this study. The loci $\Delta\mu/\Delta\mu_{spin}=0.1$ (–––) and 0.5 (---) are shown, as is the liquid spinodal (–·–).

and (P,T) planes where $\Delta\mu/\Delta\mu_{spin}=0.1$ and 0.5. According to Fig. 3, when $\Delta\mu/\Delta\mu_{spin}=0.1$, there is a 5% difference between the DFT and CNT free energy barriers. The condition $\Delta\mu/\Delta\mu_{spin}=0.5$, on the other hand, corresponds to the minimum in density at the center of critical bubble (Fig. 8), and also to the point beyond which the normalized interfacial thickness begins to grow.

IV. CONCLUSIONS

We have studied the structure and energetics of critical bubbles in the stretched Lennard-Jones fluid, using density-functional theory. The interfacial thickness, size of the critical bubble, barrier height, ratio of DFT to classical barrier heights, and average bubble density exhibit scaling behavior, in that calculations at different temperatures collapse onto a single curve when the extent of penetration into the coexistence region is normalized by the distance between the binodal and liquid spinodal, $0<\Delta\mu/\Delta\mu_{spin}<1$. Classical behavior is predicted for modest degrees of metastability: the gas–liquid interface is sharp and the bubble density resembles that of the saturated vapor. Nonclassical behavior becomes progressively evident when $\Delta\mu/\Delta\mu_{spin}$ increases: the interface becomes more diffuse, and the vapor density inside the bubble increases, becoming gradually liquidlike. For $\Delta\mu/\Delta\mu_{spin}<0.5$, the normalized interfacial thickness is virtually constant, and the density at the center of the bubble decreases as $\Delta\mu/\Delta\mu_{spin}$ increases. Both the interfacial thickness and the density at the bubble center increase beyond $\Delta\mu/\Delta\mu_{spin}=0.5$. We have also shown that the ratio of DFT to classical barrier heights has the same theoretical dependence on $\Delta\mu/\Delta\mu_{spin}$ as predicted for droplet nucleation, if the same plausible but ad hoc assumption is invoked regarding the vanishing of both sides of Eq. (13) as was made in the original derivation for droplet nucleation.[34]

Two interesting questions emerge from this work. First, it appears worthwhile to investigate the functional forms of $f(\Delta\mu,\Delta n^*)$ needed to force agreement with DFT-predicted barrier heights (Fig. 14). Secondly, our work suggests that the ratio $\Delta\mu/\Delta\mu_{spin}$ should emerge as a natural parameter in the correlation of data and in the development of improved theories of bubble nucleation in superheated liquids. In particular, the scaling with respect to $\Delta\mu/\Delta\mu_{spin}$ implies that measurements of, e.g., the nucleation rate as a function of supersaturation at a single temperature can be used to predict the nucleation rate at other conditions provided an accurate equation of state is available.

ACKNOWLEDGMENTS

The financial support of the U.S. Department of Energy, Division of Chemical Sciences, Office of Basic Energy Sciences (Grant No. DE-FG02-87ER13714). The authors are also grateful to X. C. Zeng for helpful discussions regarding the DFT calculations.

[1] P. G. Debenedetti, *Metastable Liquids* (Princeton University Press, Princeton, 1996).
[2] D. H. Trevena, *Cavitation and Tension in Liquids* (Adam Hilger, Bristol, 1987).
[3] D. F. Gaitan, L. A. Crum, R. A. Roy, and C. C. Church, J. Acoust. Soc. Am. **91**, 3166 (1992).
[4] R. C. Reid, Am. Sci. **64**, 146 (1976).
[5] R. C. Reid, Adv. Chem. Eng. **12**, 105 (1983).
[6] P. A. Lush, J. Fluid Mech. **135**, 373 (1983).
[7] C. C. Wu and P. H. Roberts, Phys. Rev. Lett. **70**, 3424 (1993).
[8] W. C. Moss, D. B. Clarke, W. W. White, and D. A. Young, Phys. Fluids **6**, 2979 (1994).
[9] D. L. Katz and C. M. Sliepcevich, Hydrocarbon Process. **50**, 240 (1971).
[10] M. Blander and J. L. Katz, Am. Inst. Chem. Eng. Symp. Ser. **21**, 833 (1975).
[11] R. C. Reid, Chem. Eng. Ed. **12**, 60 (1978).
[12] R. C. Reid, Science **203**, 1263 (1979).
[13] R. Becker and W. Doring, Ann. Phys. (Leipzig) **24**, 719 (1935).
[14] F. H. Stillinger, Phys. Rev. E **52**, 4685 (1995).
[15] I. Kusaka and D. W. Oxtoby, J. Chem. Phys. **110**, 5249 (1999).
[16] B. Senger, P. Schaaf, D. S. Corti, R. Bowles, J. C. Voegel, and H. Reiss, J. Chem. Phys. **110**, 6421 (1999).
[17] J. S. van Duijneveldt and D. Frenkel, J. Chem. Phys. **96**, 4655 (1992).
[18] V. K. Shen and P. G. Debenedetti, J. Chem. Phys. **111**, 3581 (1999).
[19] I. Kusaka and D. W. Oxtoby, J. Chem. Phys. **111**, 1104 (1999).
[20] D. W. Oxtoby and R. Evans, J. Chem. Phys. **89**, 7521 (1988).
[21] T. V. Ramakrishnan and M. Yussouff, Phys. Rev. B **19**, 2775 (1979).
[22] A. D. J. Haymet and D. W. Oxtoby, J. Chem. Phys. **74**, 2559 (1981).
[23] P. Harrowell and D. W. Oxtoby, J. Chem. Phys. **80**, 1639 (1983).
[24] X. C. Zeng and D. W. Oxtoby, J. Chem. Phys. **94**, 4472 (1991).
[25] D. J. Lee, M. M. Telo da Gama, and K. E. Gubbins, J. Chem. Phys. **85**, 490 (1986).
[26] J. D. McCoy, S. J. Singer, and D. Chandler, J. Chem. Phys. **87**, 4853 (1987).
[27] C. Seok and D. W. Oxtoby, J. Chem. Phys. **109**, 7982 (1998).
[28] V. Talanquer and D. W. Oxtoby, J. Chem. Phys. **112**, 851 (2000).
[29] X. C. Zeng and D. W. Oxtoby, J. Chem. Phys. **95**, 5940 (1991).
[30] A. Laaksonen and D. W. Oxtoby, J. Chem. Phys. **102**, 5803 (1995).
[31] Y. C. Shen and D. W. Oxtoby, J. Chem. Phys. **104**, 4233 (1996).
[32] X. C. Zeng, D. W. Oxtoby, and E. Cheng, J. Chem. Phys. **104**, 3726 (1996).
[33] M. A. Hooper and S. Nordholm, J. Chem. Phys. **87**, 675 (1987).
[34] R. McGraw and A. Laaksonen, Phys. Rev. Lett. **76**, 2754 (1996).
[35] V. Talanquer, J. Chem. Phys. **103**, 9957 (1997).
[36] P. G. Debenedetti and H. Reiss, J. Chem. Phys. **108**, 5498 (1998).
[37] J. W. Gibbs, *The Scientific Papers of J. Willard Gibbs* (Dover, New York, 1961), Vol I.
[38] J. P. Hirth and G. M. Pound, *Condensation and Evaporation: Nucleation and Growth Kinetics* (MacMillan, New York, 1963).
[39] D. Kashchiev, J. Chem. Phys. **76**, 5098 (1982).
[40] K. Koga and X. C. Zeng, J. Chem. Phys. **110**, 3466 (1999).
[41] D. W. Oxtoby and D. Kashchiev, J. Chem. Phys. **100**, 7665 (1994).

[42] D. W. Oxtoby, in *Fundamentals of Inhomogeneous Fluids*, edited by D. Henderson (Marcel Dekker, New York, 1992), Chap. 10.
[43] M. M. Telo da Gama and R. Evans, Mol. Phys. **43**, 229 (1983); **43**, 251 (1983).
[44] N. F. Carnahan and K. E. Starling, J. Chem. Phys. **51**, 635 (1969).
[45] J. D. Weeks, D. C. Chandler, and H. C. Andersen, J. Chem. Phys. **54**, 5237 (1971).
[46] B. Q. Lu, R. Evans, and M. M. Telo da Gama, Mol. Phys. **55**, 1319 (1985).
[47] J. S. Rowlinson and B. Widom, *Molecular Theory of Capillarity* (Oxford, New York, 1989).